

# Three-dimensional shape measurement with a fast and accurate approach

Zhaoyang Wang,<sup>1,\*</sup> Hua Du,<sup>1</sup> Seungbae Park,<sup>2</sup> and Huimin Xie<sup>3</sup>

<sup>1</sup>Department of Mechanical Engineering, Catholic University of America, Washington, D.C. 20064, USA

<sup>2</sup>Department of Mechanical Engineering, State University of New York at Binghamton, Binghamton, New York 13902, USA

<sup>3</sup>Department of Engineering Mechanics, Tsinghua University, Beijing 100084, China

\*Corresponding author: wangz@cua.edu

Received 22 October 2008; revised 5 December 2008; accepted 22 January 2009; posted 23 January 2009 (Doc. ID 103034); published 12 February 2009

A noncontact, fast, accurate, low-cost, broad-range, full-field, easy-to-implement three-dimensional (3D) shape measurement technique is presented. The technique is based on a generalized fringe projection profilometry setup that allows each system component to be arbitrarily positioned. It employs random phase-shifting, multifrequency projection fringes, ultrafast direct phase unwrapping, and inverse self-calibration schemes to perform 3D shape determination with enhanced accuracy in a fast manner. The relative measurement accuracy can reach 1/10,000 or higher, and the acquisition speed is faster than two 3D views per second. The validity and practicability of the proposed technique have been verified by experiments. Because of its superior capability, the proposed 3D shape measurement technique is suitable for numerous applications in a variety of fields. © 2009 Optical Society of America  
*OCIS codes:* 110.6880, 120.2830, 120.6660, 150.6910.

## 1. Introduction

Three-dimensional (3D) shape measurement or imaging technique for determining the 3D shape of objects has emerged as an important tool for many applications such as object detection, digital model generation, object replication, reverse engineering, rapid prototyping, product inspection, and quality control. Typical 3D shape measurement techniques, including the laser scanning method [1], the moiré method [2], the interferometry method [3], the photogrammetry method [4], the laser tracking method [5], the digital image correlation method [6], and the fringe (or structured light) projection method [7–17], mostly fall into two major categories. One category is capable of providing accurate measurements, and the other is capable of supplying fast measurements. The techniques in the former category, such as coordinate measurement and laser-based measurement

methods, are capable of providing accurate 3D shape measurements, but the measurement speeds are relatively low for whole-field measurements, because these techniques measure various points on the object sequentially. In contrast, the techniques in the fast measurement category generally yield relatively faster 3D shape measurements with lower accuracies.

As the technologies evolve, there has been a high demand for 3D shape measurement techniques to provide not only very accurate, but also very fast measurements. For example, the manufacture of many products, such as electronic components, needs an inspection and monitoring process that can measure and analyze various 3D geometric features of the products to determine whether the desired features are within the tolerance specifications. This application requires not only high measurement accuracy but also fast inspection for the following reasons: (1) measurement errors can result in erroneous inspection and further lead to an acceptable part being rejected or a defective part being

accepted, and (2) the inspection speed must match the fast manufacturing speed.

We present a noncontact, fast, accurate, low-cost, broad-range, full-field 3D shape measurement technique. Experiments show that the technique can be readily applied to numerous applications in various fields, such as product screening and quality control in manufacturing.

## 2. Existing Three-Dimensional Shape Measurement Based on Fringe Projection Profilometry

Among the existing 3D imaging and 3D shape measurement techniques, the ones based on fringe (or structured light) projection profilometry (FPP) approaches are the most widely used and are of great interest to practical applications in science and engineering [7].

A typical FPP-based 3D shape measurement system usually contains one projector unit and one or more cameras. During the 3D shape measurement, a set of fringe patterns are projected onto the surfaces of the object of interest, and the surface height/depth information will be naturally encoded into the distorted fringe patterns. Meanwhile, the object and the fringe patterns are captured by the camera(s) as digital images. By using image processing and triangulation methods, a full-field 3D point cloud representing the surfaces of the object can then be constructed. Such a FPP-based technique yields 3D shape measurements with the following features: (1) pixel-by-pixel full-field measurement, (2) relatively easy implementation, and (3) relatively fast processing. Because of these advantages, the FPP-based 3D shape measurement technique has become the most widely used technique for 3D imaging and shape measurements in academia and industry.

In spite of their popularities, most existing FPP-based 3D shape measurement techniques are typically incapable of providing measurements with both very fast speed and very high accuracy.

**Accuracy:** The original concept of the FPP-based 3D imaging and shape measurement technique was established based on using linear fringe reference carriers. In practice, however, the inherent divergent or uncollimated illumination of a projector always produces certain nonlinearities, which can bring substantial errors to the results of 3D shape determinations. To cope with this carrier nonlinearity problem, a number of techniques have been proposed. A typical scheme uses certain specific setups, where the geometric and other relevant parameters must be physically and precisely set or determined in advance. However, many of those parameters, such as the projection angle and the focal point location of a lens, are subject to excessive uncertainties in physical adjustment or measurement. Consequently, the corresponding 3D shape measurement accuracies are inevitably limited. Very recently, notable advances were made on coping with the nonlinear carrier phase functions under nonparallel

illumination for one-dimensional [18–22] and two-dimensional (2D) cases [23,24]. We present a significant extension and practical implementation of these advances for high-accuracy measurements.

**Speed:** The FPP-based 3D shape measurement techniques normally use phase-shifting schemes to perform automatic processing. The conventional techniques are mostly incapable of processing in a fast-speed manner, because the phase unwrapping and the relevant fringe order assigning issues for measurements of complex shapes are not well addressed. Only in a certain special case, where there is just one object and the object has a very simple geometric shape, can a very fast 3D measurement be performed due to the simplicity of phase unwrapping [16]. To achieve fast-speed 3D shape measurements for broad applications, this critical issue of measurement speed will be solved by the technique proposed in this paper.

In addition, due to the aforementioned nonlinearities of projection fringes and the uncertainties in specific setups, the existing techniques are not suitable for large (and small) range measurements. Furthermore, most existing techniques are incapable of measuring multiple objects and objects with complex shapes. These limitations will be lifted in the proposed technique as well.

## 3. Proposed Technique

The basic concept of the proposed technique was initially presented in a previous Letter [24]. Here we emphasize the actual implementation with a fast approach and its practical applications.

### A. System Setup

A schematic setup of the proposed 3D shape measurement technique is illustrated in Fig. 1. The measurement system is mainly comprised of a projector, a camera, and a processor unit. A continuously shifting pattern with originally straight, vertical, equally spaced fringes is projected onto the object surfaces, which are then captured by the camera. The original fringes are shown in Fig. 2 (details are introduced in Subsection 4.B). The proposed technique does not require the geometric parameters of the system setup to be physically measured or adjusted; moreover, the locations and directions of the projector and camera units can be arbitrarily set as long as the regions of interest can be illuminated and captured. In certain applications, infrared filters can be incorporated into the system to build an infrared setup to eliminate light flare.

It is evident that the proposed technique employs a generalized setup (system components can be arbitrarily positioned), which indicates a significant advancement. The generalized setup naturally allows the use of nonlinear fringe reference carriers, so the range of the measurement field can be substantially broadened, namely, from very small to very large fields of measurement.

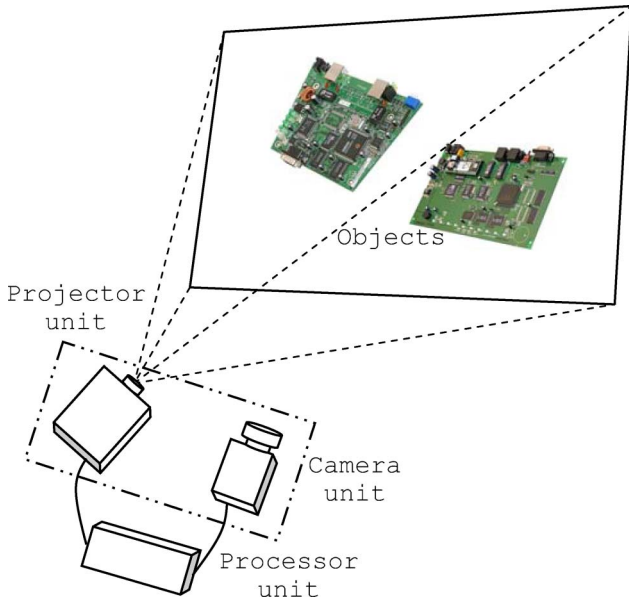


Fig. 1. (Color online) Schematic setup of the proposed technique

### B. Three-Dimensional Shape Determination

A typical 3D shape measurement requires a determination of both in-plane and out-of-plane dimension information. Since the 2D in-plane dimension can be readily determined from the corresponding digital image (upon ideal imaging without distortion) through a simple transformation when the object-camera distances are known, the technical interest actually focuses on the out-of-plane dimension measurement (it provides the location and distance information as well). Accordingly, the primary task of the proposed technique is to accurately determine the out-of-plane dimension, i.e., height and depth, in a fast-speed manner.

Figure 3 illustrates the geometric relationship of the proposed system [24], where the reference plane  $Oxy$ , the camera imaging plane  $O'x'y'$ , and the projection plane  $O''x''y''$  are arbitrarily arranged. In Fig. 3,  $P$  represents an arbitrary point on the object,  $B$  indicates the imaging point of  $P$ ,  $D$  indicates the original fringe point projected at  $P$ , and  $A$  and  $C$  denote the lens centers, the camera and projector, respectively. For convenience and clarification purposes, the coordinates of a point in a coordinate system are denoted by the corresponding coordinate symbols, and the

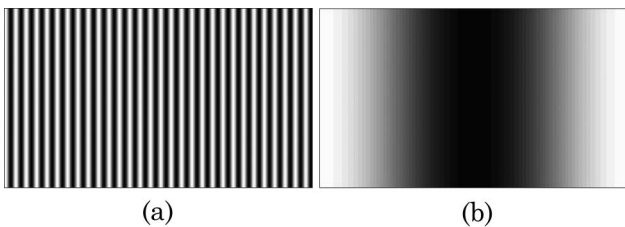


Fig. 2. Projection fringes used in the proposed technique: (a) primary high-frequency fringe pattern and (b) secondary low-frequency fringe pattern.

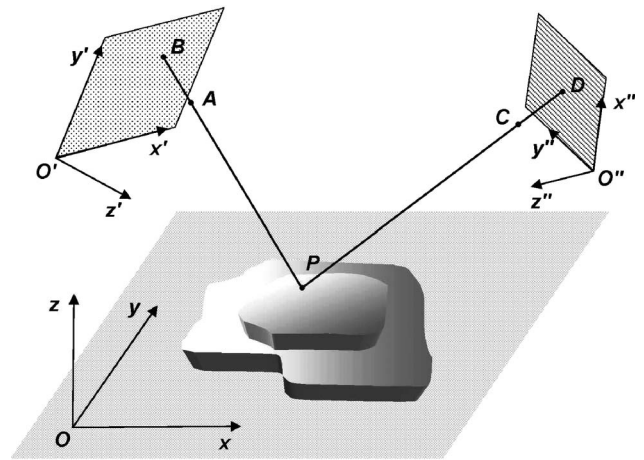


Fig. 3. Schematic of the geometric relationship in the proposed system setup

symbol of the point is chosen as the subscript. For instance, point  $P$  is denoted by  $(x_p, y_p, z_p)$ ,  $(x'_p, y'_p, z'_p)$ , and  $(x''_p, y''_p, z''_p)$  in coordinate systems  $Oxyz$ ,  $O'x'y'z'$ , and  $O''x''y''z''$ , respectively.

Considering the coordinate relationship among points  $P$ ,  $A$ , and  $B$  in the system  $Oxyz$ , it is easy to get

$$\{x_P \ y_P\} = \{z_P - z_A \ z_B - z_P\} \begin{Bmatrix} x_B & y_B \\ x_A & y_A \end{Bmatrix} / (z_B - z_A), \quad (1)$$

and the relationship among points  $P$ ,  $C$ , and  $D$  yields

$$\{x_D \ y_D\} = \{z_D - z_C \ z_P - z_D\} \begin{Bmatrix} x_P & y_P \\ x_C & y_C \end{Bmatrix} / (z_P - z_C). \quad (2)$$

A typical coordinate (affine) transformation of point  $B$  from system  $O'x'y'z'$  to system  $Oxyz$  is described as

$$\{x_B \ y_B \ z_B\} = \{x_{O'} \ y_{O'} \ z_{O'}\} + \{x'_B \ y'_B \ z'_B\} R_{\alpha,\beta,\gamma}^T, \quad (3)$$

where  $\alpha$ ,  $\beta$ , and  $\gamma$  are the sequential rotation angles about the  $x'$ ,  $y'$ , and  $z'$  axes, respectively, and  $R$  is the corresponding coordinate transformation matrix. Similarly, a coordinate transformation of point  $D$  from system  $Oxyz$  to system  $O''x''y''z''$  can be written as

$$\{x''_D \ y''_D \ z''_D\} = -\{x_{O''} \ y_{O''} \ z_{O''}\} + \{x_D \ y_D \ z_D\} R_{\theta,\phi,\psi}^T, \quad (4)$$

where  $\theta$ ,  $\phi$ , and  $\psi$  are the sequential rotation angles about the  $x$ ,  $y$ , and  $z$  axes, respectively. From Fig. 3 it is clear that, in Eqs. (3) and (4),  $z'_B = 0$  and  $z''_D = 0$ .

The fringe phase  $\Phi_B$  at point  $B$  must be identical with the fringe phase  $\Phi_D$  at point  $D$ , and this gives

$$\Phi_B = \Phi_B(x'_B, y'_B) = \Phi_D(x''_D, y''_D) = \Phi_{O'} + 2\pi x''_D/p. \quad (5)$$

Here  $p$  is the pitch of the original projection fringes. Substituting Eqs. (1)–(4) into Eq. (5) yields a complicated equation that can be simplified as

$$z_P = \frac{1 + c_1\Phi_B + (c_2 + c_3\Phi_B)x'_B + (c_4 + c_5\Phi_B)y'_B}{d_0 + d_1\Phi_B + (d_2 + d_3\Phi_B)x'_B + (d_4 + d_5\Phi_B)y'_B}. \quad (6)$$

The coefficients  $c_1$ – $c_5$  and  $d_0$ – $d_5$  are constants determined by the geometric and other relevant parameters, including  $x_A, y_A, z_A, x_C, y_C, z_C, x_{O'}, y_{O'}, z_{O'}, \alpha, \beta, \gamma, \theta, \phi, \psi, p$ , and  $\Phi_{O'}$ . Since there is a direct linear relationship between coordinates  $(x'_B, y'_B)$  in the  $O'x'y'$  system and pixel coordinates  $(I_B, J_B)$  in the captured digital image, Eq. (6) can be rewritten in terms of pixel coordinates as

$$z_P = \frac{1 + C_1\Phi_B + (C_2 + C_3\Phi_B)I_B + (C_4 + C_5\Phi_B)J_B}{D_0 + D_1\Phi_B + (D_2 + D_3\Phi_B)I_B + (D_4 + D_5\Phi_B)J_B}. \quad (7)$$

To calculate the absolute out-of-reference-plane height  $z_p$  with Eq. (7), the coefficients  $C_1$ – $C_5$  and  $D_0$ – $D_5$ , which are functions of the aforementioned geometric and other relevant parameters, must be determined first. Since physically measuring those parameters should be avoided to ensure high measurement accuracy and practicability, the coefficients will be determined through using a least-squares inverse approach based on the reference plane and one or more gauge blocks whose heights are precisely known. The reference plane and the gauge objects are used for the system calibration (i.e., determination of the coefficients) only; they are not required in actual 3D shape measurements. The least-squares error can be expressed as

$$S = \sum_{i=1}^m \left[ \frac{1 + C_1\Phi_i + (C_2 + C_3\Phi_i)I_i + (C_4 + C_5\Phi_i)J_i}{D_0 + D_1\Phi_i + (D_2 + D_3\Phi_i)I_i + (D_4 + D_5\Phi_i)J_i} z_i^g \right]^2, \quad (8)$$

where  $z_i^g$  denotes the absolute out-of-reference-plane heights of the reference plane (height is zero) and gauge blocks,  $i$  is the ordinal number of each datum point,  $m$  is the total number of datum points on the reference plane and gauge blocks used in the calculation, and a larger  $m$  generally yields a higher accuracy. The coefficients in the equation can be determined using a conventional linear algorithm after converting the nonlinear least-squares error into a linear format. During the system calibration, coefficients  $C_1$ – $C_5$  are calculated based on the reference plane of height zero, and coefficients  $D_0$ – $D_5$  are determined using two or more gauge objects of uniform

but different heights (or a one gauge object with varying heights).

#### 4. Implementation

The proposed 3D shape measurement technique employs a generalized setup that does not need a system adjustment, and the proposed governing equation is very simple; consequently, it should be easy to carry out an accurate 3D shape measurement with this technique. In practice, one problem that will arise is how to obtain the unwrapped whole-field phase distributions, i.e.,  $\Phi$  in Eqs. (7) and (8), from real projection fringe patterns.

In most of the existing FPP-based measurement techniques, a conventional phase-shifting scheme is adopted. To extract full-field phase distributions, the conventional phase-shifting analysis requires a specific number of fringe images with specific phase-shift amounts; therefore a well-designed synchronization between projecting fringes and capturing images is obligatory. Moreover, to correctly obtain the desired unwrapped phases, most existing techniques require the object being measured to be a single object of relatively simple shape. In reality, however, there are normally multiple objects in the field of view, and the objects may have complex shapes. To cope with this essential problem, a random phase-shifting scheme and a multifrequency fringe projection approach are employed in the implementation of the proposed technique.

##### A. Phase Shifting

The proposed technique utilizes a random phase-shifting scheme [25,26], which can accurately analyze phase-shifted fringe patterns even though the phase shifts are completely arbitrary. It is noteworthy that the random phase-shifting scheme can handle any number of fringe images as long as three or more of the images involve different phase-shift amounts. For this reason, the proposed technique allows the projection fringes to shift by any amount at any speed and the camera to capture the phase-shifted images at any speed (such as real time) during the 3D shape measurement. In other words, the projector unit and the camera unit can be fully independent. This is a fundamental advancement over the existing techniques that rely on synchronization among different components of the system. The introduction of the random phase-shifting scheme significantly reduces the strict requirements on hardware and software implementations. This makes the accurate and fast 3D shape measurements more powerful and feasible for practical applications.

It may be helpful to point out that, in applications where only high accuracy is demanded and measurement speed is not a concern, the projection and capture procedures can be performed in conventional ways; in this case, the classic phase-shifting scheme can always be adopted in the measurement.

## B. Phase Determination: Phase Unwrapping

In general applications, where there are multiple separated objects of interest and/or the object(s) has a complex shape, the fringe orders on each object and among different objects are often discontinuous. For a precise phase determination, such discontinuities of fringe orders must be correctly detected. This task can be accomplished by algorithms based on temporal neighborhood unwrapping, and such algorithms include temporal unwrapping and hierarchical unwrapping [27–33]. In the proposed technique, a multifrequency fringe projection approach based on these algorithms is employed. The approach employs both high-frequency fringes (e.g., tens of fringes in the field) and low-frequency fringes (e.g., one fringe in the field), as shown in Fig. 2, to automatically determine the full-field phase distributions in an ultrafast manner. The approach is described as follows.

The lowest-frequency fringe pattern with one single fringe in the entire field can yield full-field phase distributions without a phase-unwrapping process. The accuracies of such single-fringe-determined phase distributions are insufficient for being directly used in accurate 3D shape constructions; however, they can provide the required integer fringe order offsets for the fringes of higher frequency. Consequently, the unwrapped phase distributions of the higher frequency fringes can be readily calculated without a general phase unwrapping, no matter how complex the fringe patterns are. This approach can be expressed as

$$\Phi_i^{uw} = \Phi_i^w + \text{INT} \left( \frac{\Phi_{i-1}^{uw} \cdot \frac{f_i}{f_{i-1}} - \Phi_i^w}{2\pi} \right) \cdot 2\pi \quad (9)$$
$$(i = 1, 2, \dots, n),$$

where the subscript  $i$  indicates the  $i$ th projection fringe pattern, and the superscripts  $uw$  and  $w$  denote unwrapped phase and wrapped phase, respectively. In the equation,  $n \geq 1$ , the number of fringe frequencies is  $n + 1$ ,  $f$  is the relative fringe frequency or the number of fringes in the projection pattern,  $f_n > f_{n-1} > \dots > f_0 = 1$ , INT represents an operator to take the rounding integer of a decimal number, the wrapped phase distributions  $\Phi^w$  are obtained from the aforementioned phase-shifting scheme, and the initial condition is  $\Phi_0^{uw} = \Phi_0^w$ .

The algorithm is a simplified extension of the existing temporal unwrapping and hierarchical unwrapping algorithms [27–33], which are very effective in general applications such as digital holography and FPP. Since the simplified algorithm involves only a single governing equation, i.e., Eq. (9), and it can handle arbitrary fringe frequencies, the algorithm is very easy to use. The robustness in practice has been verified by all the tests conducted, as can be seen in Section 5.

Unlike the conventional, time-consuming phase-unwrapping process adopted in many FPP-based 3D shape measurement techniques, the direct

phase-unwrapping approach based on multifrequency fringe projection can obtain full-field unwrapped phase distributions in an ultrafast manner; in addition, the novel approach makes practically measuring multiple objects with complex shapes applicable. During the 3D shape measurements, the multifrequency fringes are projected alternately, and the camera continuously captures the 2D images of the objects and the fringe patterns. A certain number (e.g., three) of newest images for each pattern of different fringe frequencies are identified, kept, and updated in computer memory for constructing 3D shapes. In this way, the process of projecting fringes, capturing images, and analyzing images/data can be performed simultaneously in a parallel mode, which is essential for fast 3D shape measurement.

## C. Other Considerations

To achieve high measurement accuracies, the lens distortions of the camera and the projector are considered, and the corresponding camera calibration algorithm [34,35] is incorporated into the implementation of the proposed technique.

It is noted that, although the technique provides measurements of the out-of-plane dimension relative to a reference plane, the reference plane does not have to physically exist in actual applications, except for the system calibration purpose; furthermore, the reference plane is not necessarily the background plane nor necessarily located behind the objects of interest. This feature indicates that a rigid-body translation and rotation of the entire camera–projector system will not affect the governing parameters or the virtual reference plane. Consequently, with regard to the convenience, the 3D shape measurement or imaging system works in a similar way as a common 2D camera.

## 5. Experiment

Experiments have been carried out to demonstrate the applicability of the proposed technique. Among the five experiments presented here, the first one aims to check the measurement accuracy of the technique, and the other four intend to show the practicability of the technique. Each of the experiments involves one or more of the following issues that could be typically encountered in practice: tilted fringes, nonlinear fringes, complex shapes, multiple objects, and large areas of measurement. As previously described, these issues make the existing techniques not ideal for the corresponding 3D shape measurements, whereas they can be well addressed by the proposed technique. Detailed accuracy analysis and simulation comparison have been reported in the authors' previous work [24].

In each of the five independent experiments, the camera and the projector are arbitrarily positioned according to the generalized setup. In the measurements, five different fringe frequencies are adopted, as described in detail later, and three or four different frames of images are used for each case. Thus

15–20 frames of images are actually employed to perform a single-view 3D shape measurement. The camera delivers 60 frames/s at  $768 \times 576$  pixel resolution with Camera Link standard. For the first four measurements, two Mitutoyo gauge blocks of heights  $6.35 \pm 0.0003$  and  $25.40 \pm 0.0004$  mm were employed to calibrate the measurement system. In the last experiment, two large plates of heights  $3.175 \pm 0.003$  and  $6.35 \pm 0.006$  mm served as the gauge objects.

#### A. Accuracy Examination

A block of height  $15.24 \pm 0.0003$  mm is tested for the accuracy examination. Five different fringe frequencies, with 1, 2, 8, 40, and 160 fringes, respectively, contained in the projection images, are used in the experiment. This gives  $n = 4$ ,  $f_0 = 1$ ,  $f_1 = 2$ ,  $f_2 = 8$ ,  $f_3 = 40$ , and  $f_4 = 160$  in Eq. (9). Figures 4(a) and 4(b) show two representative images with randomly phase-shifted projection fringes of 2 and 160 fringes in the entire field (it is noted that the images have been cropped). Figures 4(c) and 4(d) are the experimentally determined 2D and 3D shape maps. The maximum and minimum heights on the block surface relative to the reference plane, against which the block is firmly placed, are detected to be 15.265 and 15.215 mm, respectively. This yields a difference of  $\pm 0.025$  mm from the actual height and reveals a high accuracy of measurement with an error of 0.16%. Since the 3D shape is obtained from the conventional 2D images, the measurement error of the out-of-plane height or depth is highly related to the in-plane resolutions. Consequently, the relative accuracy, defined as the ratio of out-of-plane measurement accuracy to the in-plane dimension, is more meaningful in assessing the measurement capability. Considering that the original width of the image is  $250 \pm 1$  mm, as shown in Fig. 4(e), the relative accuracy can thus be determined to be approximately 1/10,000. With regard to the measurement speed, it took less than 0.5 s during the experiments to complete one view of the 3D shape measurement with a regular personal computer. The result verifies that the proposed technique is capable of measuring the 3D shape of objects with high accuracies in a fast manner.

#### B. Practicability Examination: Applications

The practicability of the proposed technique has been demonstrated by four applications. In the first three experiments, five sets of projection patterns with 1, 2, 4, 20, and 40 fringes in the field are employed. It is noted that the maximum number of fringes in the field is lower than the one in previous experiments, because the entire field is smaller; the absolute fringe frequencies, in terms of number of fringes per pixel, are actually similar. In the fourth measurement, projection patterns with 1, 3, 9, 36, and 72 fringes in the field are adopted. It is important to point out that the experiments can use a different number of fringe frequencies instead of 5 and can use projection fringes with frequencies higher than

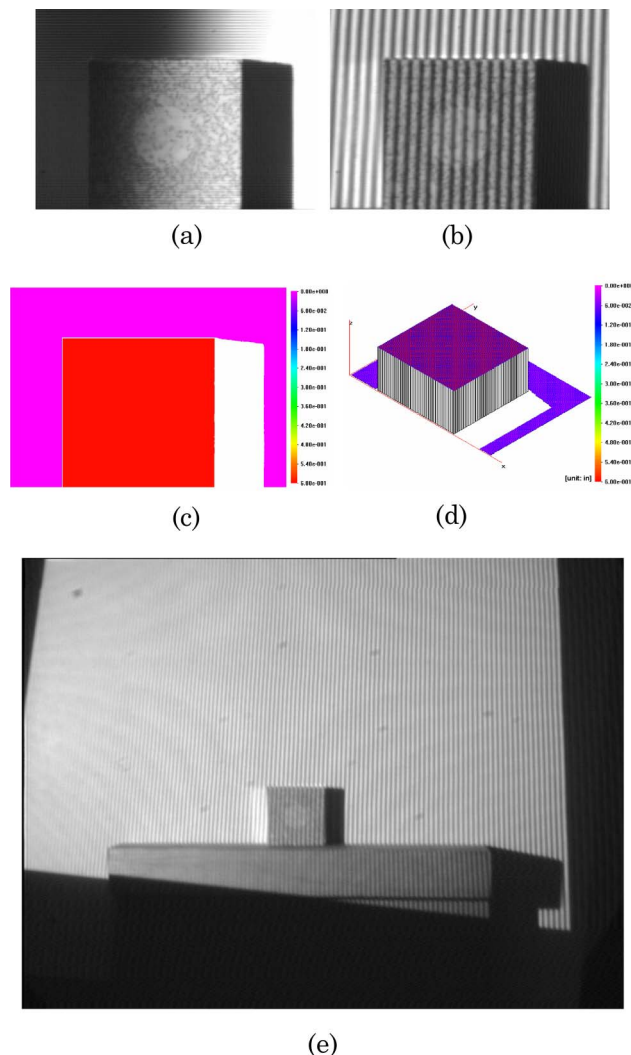


Fig. 4. (Color online) Accuracy examination: (a) low-frequency fringe pattern, (b) high-frequency fringe pattern, (c) 2D shape map, (d) 3D shape map, and (e) original and uncropped image.

40 or 72. A corresponding study on rigorously optimizing the selection of fringe frequencies is challenging and has not been performed; it will be a part of future work. In all four experiments, like the previous one, the 3D shape measurement of each view took less than 0.5 s to complete.

The first experiment involves measuring the 3D shape of a printed circuit board (PCB). Figures 5(a) and 5(b) show two fringe patterns captured during the measurement. Figure 5(c) is the 2D shape map, and Fig. 5(d) shows the 3D rendered shape map.

The second application is to simultaneously measure the 3D shapes of multiple objects, which are shown in Fig. 6(a). Figure 6(b) is a typical image captured in the experiment, and the experimentally determined 2D and 3D shapes of objects are shown in Figs. 6(c) and 6(d), respectively.

The proposed 3D shape measurement technique has also been employed to construct a complete  $360^\circ$  3D image of a rabbit model that has complex

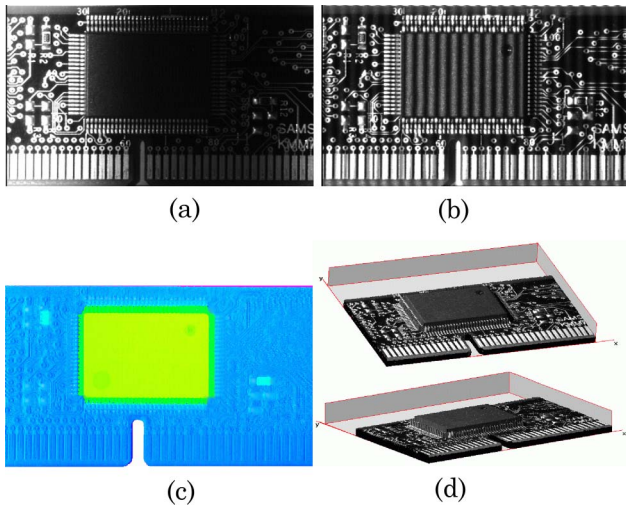


Fig. 5. (Color online) 3D shape measurement of a PCB: (a) low-frequency fringe pattern, (b) high-frequency fringe pattern, (c) 2D shape map, and (d) 3D rendered shape map.

and very rough surface shapes. Moreover, the model is very dark in color, which is quite challenging to the 3D shape measurement techniques without using phase-shifting schemes. In this application, the 3D shapes of the rabbit model at five different views are determined first; they are then connected together to form a complete 360° 3D image. Figure 7(a) shows three representative images captured from the same view, and Fig. 7(b) illustrates the constructed complete 360° 3D image. Unlike the case in the existing techniques that require the fringe carriers on the reference plane to be vertical and uniform, it is evident from the figure that arbitrarily inclined fringe carriers are used in the experiment.

Finally, the proposed technique is employed to inspect the 3D shape of a transparent Plexiglas plate, which is covered by papers and tapes except for the

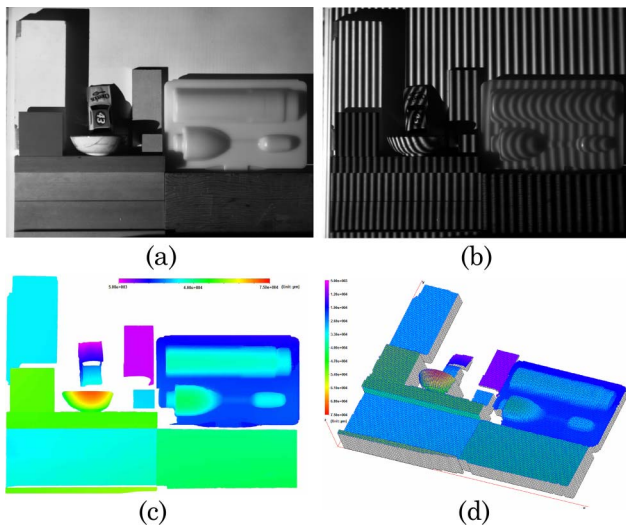


Fig. 6. (Color online) 3D shape measurements of multiple objects: (a) objects, (b) a typical fringe image, (c) 2D shape map, and (d) 3D shape map.

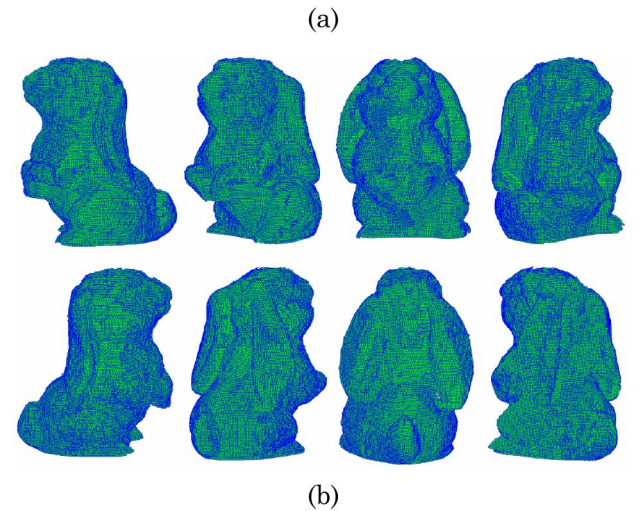
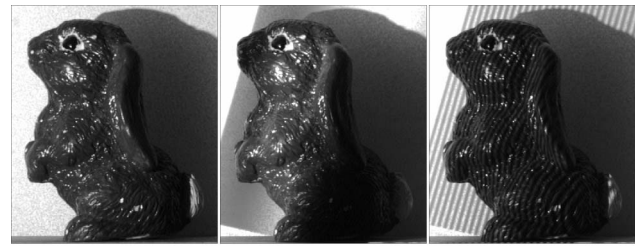


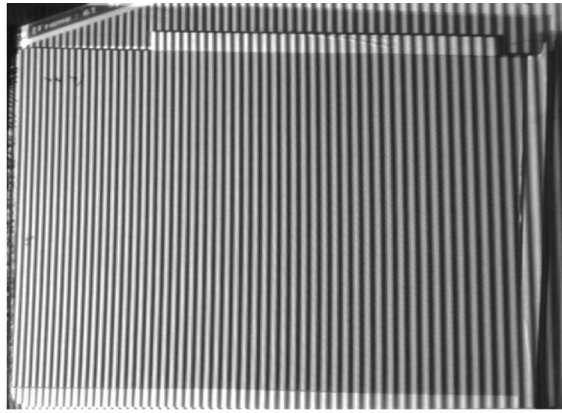
Fig. 7. (Color online) 3D shape measurement of a rabbit model: (a) three representative fringe patterns from the same view and (b) illustration of the complete 360° 3D image.

top and right areas. The size of the paper- and tape-covered region is approximately 718 mm by 508 mm. Figure 8(a) is a representative image captured, where the fringe nonuniformity is evident. Since the top and right regions are transparent, the fringes there are actually located on a board behind the Plexiglas plate. Consequently, those regions are excluded in the detected 2D and 3D shapes, as shown in Figs. 8(b) and 8(c). In the 3D plot, the out-of-plane warpage has been magnified for visualization purpose.

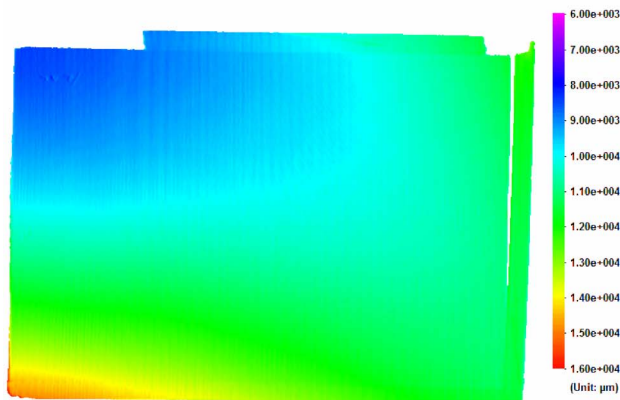
The results from these applications have effectively verified the practicability of the proposed technique.

## 6. Discussion: Accuracy, Speed, and Other Features

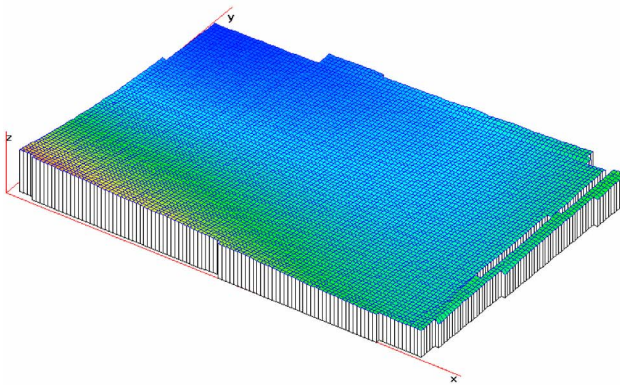
Since the in-plane dimension is directly provided by the 2D image and the out-of-plane dimension (which is of more interest) is determined through calculations based on image/data analysis, the terms *relative resolution* and *relative accuracy* are typically used to describe the in-plane and out-of-plane measurement capabilities, respectively. The (in-plane) relative resolution is inherently governed by the image resolution; for instance, it is 1/1024 for an image of 1024 × 1024 pixels. The resolution can be enhanced by numerical interpolation if applicable and necessary. The (out-of-plane) relative accuracy is defined as the ratio of absolute out-of-plane measurement accuracy to the actual in-plane dimension, and it is usually higher than the relative resolution, because



(a)



(b)



(c)

Fig. 8. (Color online) 3D shape measurement of a Plexiglas plate: (a) a representative fringe image, (b) 2D shape map, and (c) 3D shape map.

the corresponding calculation is not limited to pixel resolution for the out-of-plane dimension determination. In the accuracy examination experiment previously presented, a relative accuracy of approximately  $1/10,000$  has been confirmed. In the practicability examination measurements, since the authors do not have a more accurate tool than the proposed technique to measure the dimensions, the exact errors were not given in order to avoid misleading.

With the proposed camera–projector-independent setup, random phase shifting, ultrafast phase unwrapping based on multifrequency fringe projection, and direct 3D shape calculation approaches, the proposed technique is capable of achieving a speed higher than two 3D views per second for broad 3D shape measurements in practice. It is understood that, if there is only one object in the field of view and the object has a very simple geometric shape, the existing technique based on phase subtraction algorithm can provide faster speed [16] (with lower accuracy though, due to the aforementioned uncertainties in real application). For general applications that involve multiple objects or a single object with complex shapes, the conventional techniques must rely on human–computer interactions to assign correct fringe order offsets in different regions first before unwrapping a complex phase map. Consequently, the existing techniques based on a conventional phase-unwrapping scheme are incapable of measuring 3D shapes in a fast manner. For instance, it could take up to 1 h or more to obtain a correct full-field unwrapped phase map for the fringe image shown in Fig. 6(b), because identifying the fringe order offsets in all regions are very difficult and time-consuming.

It may be worth noting that numerous papers on 3D shape measurement and 3D imaging have been published in the past two decades. To justify the proposed work, in addition to a general literature survey, the authors have carefully completed a thorough literature survey on the relevant 3D shape measurement and imaging work published in tens of technical journals within the past five years. In terms of combined technical features, which include but are not limited to low cost (\$2000), high accuracy ( $1/10,000$ ), fast speed (two 3D images/s), capability of measuring multiple and complicated objects, and easy-to-implement (no adjustment or tune-up is required other than calibration), the authors did not notice any existing work capable of providing substantially better features than the proposed technique.

During the research, the authors also identified most of the industrial/commercial products on fast and accurate 3D shape measurement and imaging. At present, there are a couple of commercial 3D shape measurement products capable of providing similar accuracy and speed as the ones of the presented technique. However, the commercial products are very expensive, and the technical details are unclear. For the experimental implementation work of this paper, low-cost camera and projector units (totaling less than \$2000) are used. It is expected that the measurement accuracy could be further enhanced when high-quality components, which provide images with high signal-to-noise ratio and low image distortion, are employed. It is also noteworthy that five different fringe frequencies are selected to ensure correct full-field phase determinations in all the experiments conducted. With

high-quality camera and projector components, fewer number of frequencies can be used to improve the measurement speed; in addition, optimizing the algorithms and program codes with a multithread approach can also significantly reduce the processing time and enhance the measurement speed. These issues, together with the investigation of the fringe frequencies selection, will be considered in future work. It is reasonable to assume that a relative accuracy of higher than 1/10,000 and a speed of faster than five 3D views per second should be quite conservative for the proposed technique in future applications.

## 7. Conclusion

A noncontact, fast, accurate, low-cost, broad-range, full-field, easy-to-implement 3D shape measurement technique is presented. The technique is based on a generalized setup that needs neither a specific arrangement of components nor a system adjustment, so the cost is very low (less than \$2000), and the technique is quite easy to implement. With the great promise of effectively handling the various uncertainties in practice and coping with the typical limitations in conventional techniques, the new technique is capable of measuring the 3D shape of multiple objects with complex shapes, and the field of view can be very broad, i.e., from very small to very large fields. The measurement accuracy can reach a relative accuracy of 1/10,000 or higher, and the acquisition speed is faster than two 3D views per second. The validity and the practicability of the proposed technique have been verified by experiments.

Because of its superior capability, the proposed technique is suitable for numerous applications in many fields where fast and accurate 3D image or shape construction is required, such as object detection, digital model generation, object replication, reverse engineering, rapid prototyping, product inspection, and quality control. The technique may also serve as an experimental tool to investigate the deformation involved in a variety of mechanics analysis.

This work was supported by a Burns Fellowship at the Catholic University of America, the National Collegiate Inventors and Innovators Alliance, under grant 5205-07, and the National Science Foundation (NSF), under grant 0825806.

## References

1. C. Keferstein and M. Marxer, "Testing bench for laser triangulation sensors," *Sens. Rev.* **18**, 183–187 (1998).
2. T. Yoshizawa and T. Tomisawa, "Shadow moiré topography by means of the phase shift method," *Opt. Eng.* **32**, 1668–1674 (1993).
3. C. Wagner, W. Osten, and S. Seebacher, "Direct shape measurement by digital wavefront reconstruction and wavelength scanning," *Opt. Eng.* **39**, 79–85 (2000).
4. C. Fraser, "Photogrammetric measurement to one part in a million," *Photogramm. Eng. Remote Sens.* **58**, 305–310 (1992).
5. S. Kyle, R. Loser, and D. Warren, "Automated part positioning with the laser tracker," in *Proceedings of the Fifth International Workshop on Accelerator Alignment*, ANL/FNAL (1997).
6. S. McNeill, M. Sutton, Z. Miao, and J. Ma, "Measurement of surface profile using digital image correlation," *Exp. Mech.* **37**, 13–20 (1997).
7. F. Chen, G. Brown, and M. Song, "Overview of 3-D shape measurement using optical methods," *Opt. Eng.* **39**, 10–22 (2000).
8. W. Schreiber and G. Notni, "Theory and arrangements of self-calibrating whole-body 3-D measurement systems using fringe projection technique," *Opt. Eng.* **39**, 159–169 (2000).
9. L. Salas, E. Luna, J. Salinas, V. Garcia, and M. Servin, "Profilometry by fringe projection," *Opt. Eng.* **42**, 3307–3314 (2003).
10. Q. Hu, P. Huang, Q. Fu, and F. Chiang, "Calibration of a three-dimensional shape measurement system," *Opt. Eng.* **42**, 487–493 (2003).
11. R. Legarda-Sáenz, T. Bothe, and W. Juptner, "Accurate procedure for the calibration of a structured light system," *Opt. Eng.* **43**, 464–471 (2004).
12. C. Tay, C. Quan, T. Wu, and Y. Huang, "Integrated method for 3-D rigid-body displacement measurement using fringe projection," *Opt. Eng.* **43**, 1152–1159 (2004).
13. T. Peng, S. Gupta, and K. Lau, "Algorithms for constructing 3-D point clouds using multiple digital fringe patterns," *Comput. Aided Des. Appl.* **2**, 737–746 (2005).
14. J. Pan, P. Huang, and F. Chiang, "Color-coded binary fringe projection technique for 3-D shape measurement," *Opt. Eng.* **44**, 023606 (2005).
15. H. Guo, H. He, Y. Yu, and M. Chen, "Least-squares calibration method for fringe projection profilometry," *Opt. Eng.* **44**, 033603 (2005).
16. S. Zhang, X. Li, and S. Yau, "Multilevel quality-guided phase unwrapping algorithm for real-time three-dimensional shape reconstruction," *Appl. Opt.* **46**, 50–57 (2007).
17. S. Zhang and S. Yau, "Generic nonsinusoidal phase error correction for three-dimensional shape measurement using a digital video projector," *Appl. Opt.* **46**, 36–43 (2007).
18. L. Chen and C. Quan, "Fringe projection profilometry with nonparallel illumination: a least-squares approach," *Opt. Lett.* **30**, 2101–2103 (2005).
19. L. Chen and C. Quan, "Reply to comment on 'fringe projection profilometry with nonparallel illumination: a least-squares approach,'" *Opt. Lett.* **31**, 1974–1975 (2006).
20. Z. Wang and H. Bi, "Comments on fringe projection profilometry with nonparallel illumination: a least-squares approach," *Opt. Lett.* **31**, 1972–1973 (2006).
21. H. Du and Z. Wang, "Real-time 3-D shape measurement with high accuracy and low cost," in *Conference on Lasers and Electro-Optics/Quantum Electronics and Laser Science Conference and Photonic Application System Technologies*, OSA Technical Digest Series (CD) (Optical Society of America, 2006), paper JThD49.
22. Z. Wang, H. Du, and H. Bi, "Out-of-plane shape determination in fringe projection profilometry," *Opt. Express* **14**, 12122–12133 (2006).
23. H. Guo, M. Chen, and P. Zhang, "Least-squares fitting of carrier phase distribution by using a rational function in fringe projection profilometry," *Opt. Lett.* **31**, 3588–3590 (2006).
24. H. Du and Z. Wang, "Three-dimensional shape measurement with arbitrarily arranged fringe projection profilometry system," *Opt. Lett.* **32**, 2438–2440 (2007).
25. Z. Wang and B. Han, "Advanced iterative algorithm for phase extraction of randomly phase-shifted interferograms," *Opt. Lett.* **29**, 1671–1673 (2004).
26. Z. Wang and B. Han, "Advanced iterative algorithm for randomly phase-shifted interferograms with intra- and inter-frame intensity variations," *Opt. Lasers Eng.* **45**, 274–280 (2007).

27. C. Coggrave and J. Huntley, "High-speed surface profilometer based on a spatial light modulator and pipeline image processor," *Opt. Eng.* **38**, 1573–1581 (1999).
28. L. Kinell, "Spatiotemporal approach for real-time absolute shape measurements by use of projected fringes," *Appl. Opt.* **43**, 3018–3027 (2004).
29. J. Tian and X. Peng, "Three-dimensional vision from a multisensing mechanism," *Appl. Opt.* **45**, 3003–3008 (2006).
30. W. Osten, W. Nadeborn, and P. Andra, "General hierarchical approach in absolute phase measurement," *Proc. SPIE* **2860**, 2–13 (1996).
31. W. Nadeborn, P. Andra, and W. Osten, "A robust procedure for absolute phase measurement," *Opt. Lasers Eng.* **24**, 245–260 (1996).
32. J. Burke, T. Bothe, W. Osten, and C. Hess, "Reverse engineering by fringe projection," *Proc. SPIE* **4778**, 312–324 (2002).
33. W. Osten and P. Ferraro, "Digital holography and its application in MEMS/MOEMS inspection," in *Optical Inspection of Microsystems*, W. Osten, ed. (CRC Press, 2006), p. 351–425.
34. R. Tsai, "A versatile camera calibration technique for high accuracy 3D machine vision metrology using off-the-shelf TV cameras and lenses," *IEEE J. Robot. Autom.* **3**, 323–344 (1987).
35. Z. Zhang, "A flexible new technique for camera calibration," *IEEE Trans. Pattern Anal. Mach. Intell.* **22**, 1330–1334 (2000).